Journal of Cleaner Production 375 (2022) 134133

Contents lists available at ScienceDirect

Journal of Cleaner Production

journal homepage: www.elsevier.com/locate/jclepro

Estimating the global technical potential of building-integrated solar energy production using a high-resolution geospatial model

Gergely Molnár [a,b,*], Diana Ürge-Vorsatz [a], Souran Chatterjee [a]

[a] Department of Environmental Sciences and Policy, Central European University, Nádor utca 9, 1051, Budapest, Hungary
[b] Department of Climatology and Landscape Ecology, University of Szeged, Egyetem utca 2, 6722, Szeged, Hungary

ARTICLE INFO

Handling Editor: Prof. Jiri Jaromir Klemeš

Keywords:
Solar energy
Global and regional technical potential
PV/T technology
Geospatial modeling

ABSTRACT

The building sector is responsible for about one third of the global final energy consumption and CO_2 emission, thus it is desired to limit and replace building-related fossil energy sources to meet climate goals. In this context, the utilization of building integrated solar technology has proven to be a reliable and increasingly affordable alternative, however, there is still an immense potential remained unexplored. This study thus uses, a high-resolution, geospatial energy supply model to estimate the useable building rooftop areas across 11 regions of the World, and calculates the corresponding global and regional potential of energy production of state-of-the-art rooftop PV/T collectors over a 39-year period. Our results demonstrate that solar PV/T energy production on residential and commercial/public rooftops has enormous global potential (47.5 PWh), with the possibility of doubling by 2060. The current magnitude of potential implies that about 60% of the suitable building rooftops could be installed with PV/T collectors to offset most of the local energy demand. Regarding the future trends we found that beyond the extended building stock in large economies (e.g., China, USA and EU), the newly-built commercial buildings of developing regions (e.g., Latin America and South Asia) are modeled to have key role in realizing the estimated potential over the next decades. Our study also focuses on the geographical, temporal and building-level characteristics of energy production and concludes that rooftops in the Middle East, South and Pacific Asia have the most favorable geographical exposure for capturing solar (dominantly thermal) energy by PV/T collectors. It was found to be especially valid for months during the warm season. In regions dominated by temperate climate, the energy generation is characterized by a second maximum before the warm season, due to the peak of electricity production. At the time of the production peaks and in general annually, irrespective to regions, PV/T collectors installed on single-family roofs and retails were estimated to have the greatest potential to supply green energy for the entire building and thus likely to balance the in-situ energy consumption.

1. Introduction

The building sector is responsible for almost 31% of global final energy use and 54% of final electricity demand (Rogelj et al., 2018). Energy demand of the building sector is mainly dominated by the aggregated domestic demand for the space heating/cooling, water heating, and refrigeration. Precisely, these end-use demands consume around 40 PWh energy globally, which is over one-third of the global final energy consumption (IEA, 2020a). Thus, to achieve the Paris agreement target that is to limit the temperature rise within 1.5 °C, the domestic energy demand needs to be substantially reduced by 2050 globally. However, with the increasing rate of urbanization, which was projected to be the most intense in South Asia and Sub-Saharan Africa, would further increase the energy demand of buildings, as 75% of the global final energy use and the related CO_2 emission takes place in urbanized areas (REN21, 2021).

Reducing the building end-use demand without affecting the comfort and well-being of the occupant is a challenge. The most popular option is to decarbonize the energy system with renewables. Solar radiation provides sustainable, well-predictable, efficiently harnessable and abundant form of energy. The energy of photons, as the elementary units of sunlight, can be converted instantaneously to electricity (via photovoltaic – PV – effect) and heat using various solar panels and solar thermal collectors (Zhang et al., 2013). Besides its positive

* Corresponding author. Department of Environmental Sciences and Policy, Central European University, Nádor utca 9, 1051, Budapest, Hungary.
E-mail address: MolnarG@ceu.edu (G. Molnár).

https://doi.org/10.1016/j.jclepro.2022.134133
Received 22 February 2022; Received in revised form 9 September 2022; Accepted 12 September 2022
Available online 15 September 2022

environmental aspects (e.g., clean energy, mitigation of GHGs), the solar technology has high reliability, decreasing operation and maintenance and increasing availability (Sampaio and González, 2017). Consequently, the installed solar capacity has shown a magnificent growth (from 0.42 to 586 GW) in the last two centuries across the World (Hannah and Roser, 2020).

The more vital spread of the solar technology, on the other hand, is inhibited by such yet unresolved factors as high initial costs and lack of governmental incentives, geographical limitations and mismatch between the production and consumption (i.e., power storage problems) (El Chaar et al., 2011; Trainer, 2017). Nonetheless, with the recent advancements of solar technology, buildings can produce electric and/or thermal energy with on-site solar systems and hence, there is a need of exploration of the building sector in the light of the technological advancements. The cutting-edge building-integrated solar systems help to promote net zero buildings and can play a pivotal role in passively reducing energy demand substantially without comprising with the well-being of occupants (Urge-Vorsatz et al., 2020). Additionally, solar energy production on building surfaces can alleviate the land requirement of solar energy systems and support the use of non-competing spaces on rooftops and/or on facades (van de Ven et al., 2021). Despite these benefits, the potential for solar energy production on building surfaces, especially for global scale, remained under-researched.

The BISE model (Petrichenko, 2014; Petrichenko et al., 2019) was developed to bridge this scientific gap by simulating the technical potential of electric and thermal energy produced by PV/T collectors installed on the rooftops of residential and tertiary buildings. This model was also designed to overcome the limitations of earlier global investigations in terms of suitable rooftop area, with applying a consistent, "medium-level" spatial dataset and GIS toolboxes to estimate the global distribution of building footprints. Due to the fine spatial and temporal resolution of the model, it is suitable for depicting even sub-regional (country-level) or daily variability of the potential of PV/T-related energy production. In addition to these, the flexibility of BISE makes possible to compare the outputs with building-related global energy demand models (e.g., 3CSEP-HEB: Urge-Vorsatz et al., 2012 and BUENAS: McNeil et al., 2013) to typify regions, climate zones and building types, where the net-zero emission may technically be feasible relying only on solar PV/T production. Nevertheless, certain modules of the BISE model has not been updated in the last years, so that the latest datasets for building characteristics and trends in the PV/T technology was not incorporated.

In this study, our goal, therefore, is to upgrade the outdated modules of the BISE model and employ it to give an estimation on how much energy the PV/T collectors could produce presently on residential and tertiary building rooftops, and how this technical potential will likely to evolve across worldwide regions during the forthcoming decades. To shed light on spatiotemporal characteristics, we also aimed to assess the inter-regional and inter-annual differences of the PV/T potential. Furthermore, by estimating the specific technical potentials for each analyzed building types, we explore the possible differences in the ability of buildings in supplying solar energy and in balancing the local consumption.

2. The potential of building integrated solar production

The solar energy market is dominated by the economically most profitable PV panels, although the hybrid PV/T collectors also represent a noticeable part of the solar industry. The main advantage of these PV/T collectors (combination of PV cells and a heat absorber) related to standalone PV panels is that they utilize the waste heat generated by overheating cells and transform it to useful and consumable thermal energy (Oruc et al., 2016; Shin et al., 2020). In the meantime, remarkably lower cell temperature and enhancing electric efficiency (η_{elec}) can be achieved by exhausting heat from the module (Diwania et al., 2020).

The PV/T systems are usually characterized by the type of the collector (e.g., flat plate or concentrated) and heat removal material (e.g., air or fluid-based) (Babu and Ponnambalam, 2017). The preference of a given PV/T collector type at building level is determined by many factors, including climate, building type, local regulations, maintenance and application (Bloem et al., 2012). If solar energy is applied to provide heat for space heating systems (in tall buildings) or agricultural processes (e.g., drying crops), mostly the air collectors are favored. Otherwise, for residential space heating/cooling and hot water systems, the fluid-based design seems to be more spread (IEA, 2020b). PV/T collectors can be mounted on building rooftops, facades as well as physically integrated into the structure and material of the buildings (Building Integrated PV/T – BIPV/T). A BIPV/T system is not only capable of supplying energy to balance local consumption, but has also proven to be very effective to govern the energy performance of the building in a more sustainable direction (Yang and Athienitis, 2016).

Majority of the former studies have rather focused on the local (building or city) scale analysis of solar energy potential provided by BIPV systems. Strzalka et al. (2012) combined three-dimensional geometry modeling with photovoltaic system simulations for a residential district near Stuttgart, Germany. By creating a 3D city model from geospatial data, they estimated the shadow effects and suitable roof area (54% of the total area) for each building. It was concluded that 35% of the total annual electricity (10 700 MWh) can be supplied by PV energy production. Hong et al. (2017) also recognized the capability of GIS technique and performed a hillshade analysis to explore the influence of shading on roof area suitability. After calculating the total solar radiation on the rooftops (i.e., physical potential) in the Gangnam district of Seoul, South Korea, the authors predicted the geographical and technical potential of PV electricity generation. In their findings, the annual potential of 1 130 371 MWh was equal to 12.17% of the available solar radiation during the year. In their country-level study, Buffat et al. (2018) assessed the rooftop PV potential for Switzerland. As a result of making data intensive manipulations on building footprint and digital surface layers, the orientations, slopes and horizon angles of roofs were computed for the building stock. Using the single-diode electrical model, the mean annual rooftop PV potential was found to be 53.2 TWh, which was 91% of the total Swiss electricity consumption in 2015. The authors highlighted that, despite the similar range for the consumption and production, the high inter-annual variability of meteorological conditions can alter the gap between the two sides. Walch et al. (2020) processed 3D building cadastre and digital surface model by neural network approach and modeled different PV potentials for Switzerland. The comparison of the results of the Swiss studies indicates a difference of 218 km^2, 13.7% and 16.42 TWh in suitable rooftop area, suitability rate and annual technical potential of PV production, respectively. This case draws the attention on that the results of such analysis, even for similar study areas, can significantly vary due to the source of input data and methodological assumptions.

Considering the regional investigations, Bódis et al. (2019) made a comprehensive estimation on the PV electricity generation of the EU. With precise GIS-based preparations on high-resolution building footprint raster and reference cadastral vector datasets, the available rooftop area and the technical potential was determined to be 7935 km^2 and 0.68 PWh/year. This potential was found to be suitable for covering about the one quarter of the total electricity consumption for the EU in 2016. Of the very few global studies, Hofman et al. (2002) and Hoogwijk (2004) employed a simplified assumptions for approximating the rooftop suitability and simulating the technical potential of PV panels. More precisely, Hofman et al. (2002) used GIS (e.g., solar irradiance and population), statistical (e.g., degree of electrification and suitable roof area per inhabitant) and technological data (e.g., module efficiency), and estimated the technical potential of the global PV electricity production to be 7.7 PWh/year. In this analysis, the largest production was revealed for the USA and China with 1.69 and 1.39 PWh/year. Hoogwijk (2004) divided the calculations for centralized and decentralized

production as well as for theoretical, geographical, technical and economic potential. For the decentralized technical potential of PV production, the author found a global value 6 PWh/year, with regional maxima in the OECD Europe (1.1 PWh/year) and South Asia (0.6 PWh/year). In both research, the suitable roof area was derived by using statistical assumptions based on census or GDP data, which was regarded as a potential weakness of the methodology by Hoogwijk (2004).

In the earlier interpretation of the BISE model, Petrichenko et al. (2019) realized the shortcomings of preceding global studies, and that the GIS technique and high-granularity spatial data, as 'medium level' inputs based on the classification of Castellanos et al. (2017), can be utilized not only in local or regional but also for global assessments. The authors elaborated an overarching calculation procedure that included high-resolution input data for meteorological, technological and roof geometry parameters and gave estimations on the technical potential of PV/T collectors and the extent of solar electric and thermal energy generation. They found the global electric and thermal potential being 7.2 and 6.9 PWh by 2050. Nevertheless, Petrichenko et al. (2019) emphasized certain modeling limitations regarding the scope, input data and technical details that might have affected the uncertainties of the above results. Our purpose in this study is, therefore, to overcome some earlier limitations of the BISE model, and to inspect the effect of the methodological improvements on the modeled potential of the BIPV/T energy production.

3. Methodology

In order to overwhelm some limitations of the earlier versions of the BISE model and to incorporate the latest technological innovations, the model has been upgraded to reduce the uncertainties of the simulations and be able to obtain even more realistic outputs in terms of global solar energy potential. In this section, we present only the new methodological steps and the most vital information needed to understand the modeling framework. More details on the philosophy of the BISE model can be found in Petrichenko (2014) and Petrichenko et al. (2019).

3.1. Description of modeling framework

The modeling area consists of 11 major regions that span the entire populated area of the Earth (Fig. 1.). Among the analyzed geographical territories, Africa and Former Soviet Union have the largest, while Pacific Asia and Eastern Europe are characterized by the smallest area, with $2.22 \bullet 10^7$, $4.34 \bullet 10^6$ and $1.16 \bullet 10^6$ km^2, respectively. With mean population densities 265 and 109 people/km^2, South Asia and Western Europe contains the most urbanized and built-up areas of the regions (CIESIN, 2018). It is assumed in the BISE that these urban areas contain various types of buildings, namely single family, multifamily and tertiary (e.g., educational, hospital, hotel and restaurant, retail, office and other) buildings.

In our current modeling efforts, a 39-year long period was analyzed. We select 2022 as the first year, which is considered to be a realistic date when the energy and building sector could be restored after the pandemic crisis. With the closing year of the simulations (2060), a sufficiently long investigation period was intended to be maintained, which contains the most crucial years in terms of the transformation of the energy sector to mitigate the undesired effects of climate change.

The BISE model has three types of major inputs, including meteorological, building-related and technological parameters. As it can be found in the Supplementary Material (Tables S1–S3.), the spatial and temporal characteristics of different variables vary on a wide range. Since the BISE is a grid cell-based, geospatially resolved, high-granularity model, its spatiotemporal resolution is equal to the finest resolution of input databases. The outputs, therefore, are computed with hourly time steps and on a 100-km grid mesh, which makes the detailed and well-interpretable analysis of the technical potential of solar energy supply possible. Before allocating inputs to the dynamic computational core of the model, the raw data must be preprocessed with various GIS tools to ensure the sufficient data format and quality. In the next subsection, the major steps of the data preparation are presented.

3.2. Preparation of meteorological parameters

Instead of using the popular typical (averaged) meteorological year datasets for deriving the most crucial meteorological variables (e.g., Oloo et al., 2015; Kambezidis and Psiloglou, 2021), we account for the spatiotemporal dynamics of parameters affected by the changing climate during the simulation period. For this purpose, reanalysis data from 2015 to 2019 and climate projections are combined. The role of the reanalyzed parameters is to refine the temporality of the projected fields of climatic variables.

Because of the abundance of the available variables (Table S1.) and the sufficient spatiotemporal representation, the MERRA-2 (Modern Era Retrospective-Analysis for Research and Applications) dataset (Gelaro et al., 2017) is used as the basis of the refinement. After acquiring annual profiles for each parameter for the selected era, the five profiles were aggregated into a single curve, including the mean hourly variation of the given variable over the five years. Then the mean hourly absolute values of the profiles were transformed into hourly weights by taking the daily means of the parameters into account and by dividing the related hourly values with them. As a result, four curves were generated for each variable, along with 8760 hourly weights (c_{ijk}) and values in a typical range between 0 and 5.

The future state of the climate was estimated by modeling projections obtained from CMIP-6 (Coupled Model Intercomparison Proj-

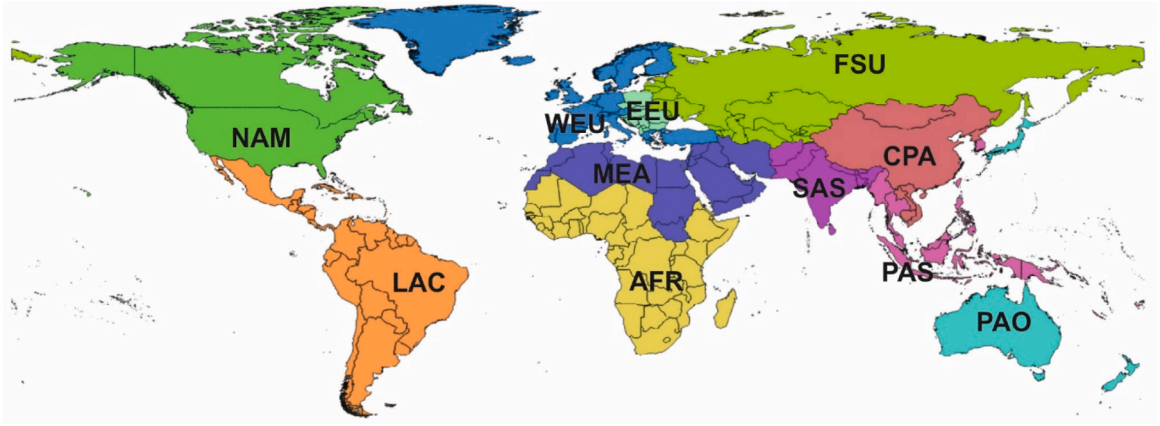

Fig. 1. Spatial distribution of modeling regions in the BISE. For the abbreviations of regions, see Table 2.

ect) database (Eyring et al., 2016). For the vast number of data products, we apply a rigorous selection process that filtered out projections with coarse grid resolution or with inadequate temporal availability. Additionally, only simulations performed with the SSP (Shared Socioeconomic Pathway) 2–4.5 scenario is taken into account. With this latter restriction, a "middle of the road" scenario was assumed in terms of CO_2 emission and global temperature rise. By introducing these filters, the number of potential modeling products was significantly reduced of which the outputs of the climate model of the Deutsches Klimarechenzentrum (Schupfner et al., 2019) are used. Since these outputs were available only at daily time step, there was a need to increase its temporality to produce the desired hourly resolution. In order to refine the time steps, the modeled daily means of each parameters were multiplied with the c_{ijk} weights derived earlier from MERRA-2 data, thus:

$$\chi_{ijk} = c_{ijk} \cdot \chi_{ij} \tag{1}$$

where χ_{ij} is the projected mean of a given variable from the DKRZ model in a month (i) and on a day (j), c_{ijk} is the hourly weight of a given variable derived from the MERRA-2 database and χ_{ijk} is the refined value of a given variable in a month, day and hour (k). Before computing Equation (1)., the c_{ijk} rasters are resampled to the resolution of χ_{ij} using Bicubic Spline resampling method. During the raster calculation process, c_{ijk} was considered as a constant layer in each i-th time step of the analysis period ($2022 \leq i \leq 2060$).

3.3. Estimation of roof area parameters

The estimation of the global pattern of roof area relied on two types of datasets (Table S2.). One of these data sources included the raster grids of Global Human Settlement Layer (GHSL) that has been produced and supported by the Joint Research Centre (JRC) and the DG for Regional and Urban Policy (DG REGIO) of the European Commission. The GHSL database consists of geospatial maps for built-up, settlement and population density information. From this dataset, we used the GHS-BUILT-S2 built-up grid system. The related raster layers were originally extracted from Sentinel-2 satellite images with convolutional neural network approach (Corbane et al., 2021). They have 10-m horizontal resolution and depict the probability of the occurrence of buildings ($0 \leq P \leq 100\%$) in a given cell. The global dataset was split into 502 regional tiles that were obtained at the Joint Research Centre Data Catalogue (JRCDC, 2020).

Since the GHS-BUILT-S2 built-up grids are not suitable to designate the real location of buildings, it was necessary to combine them with another datasets. To this end, we gathered building cadastre data for different urban areas. Building cadastre maps, being created generally from very detailed (sub-cm) aerial photographs, represent the real spatial distribution of building footprints. Consequently, such data is suitable to determine the possible threshold for P values in which the occurrence of buildings is very likely within GHS-BUILT-S2 pixels.

The cadastral maps were acquired via the INSPIRE Geoportal (INSPIRE, 2020), where a great collection of open-source data can be found. In summary, we employed nearly 6 million cadastral polygons overlaid more than 20 urban areas in Czechia (number of polygons: 24674; Geoportal ČÚZK, 2020), France (number of polygons: 4654887; ETALAB, 2020), Belgium (number of polygons: 629407; SPF FINANCES, 2020), Spain (number of polygons: 531204; IDEE, 2020) (Fig. 2.).

The first stage of the data manipulation was to harmonize the geographical coordinate reference systems of the distinct GIS data sources. Of the 502 raster tiles, we filtered out those layers that had no overlap with the cadastral data. After simultaneously merging raster layers, spatially joining cadastral polygons and combining these files into one common virtual layer, zonal statistics calculations were performed to compute the mean P values for grid cells covered by building cadastre polygons (Fig. 3.).

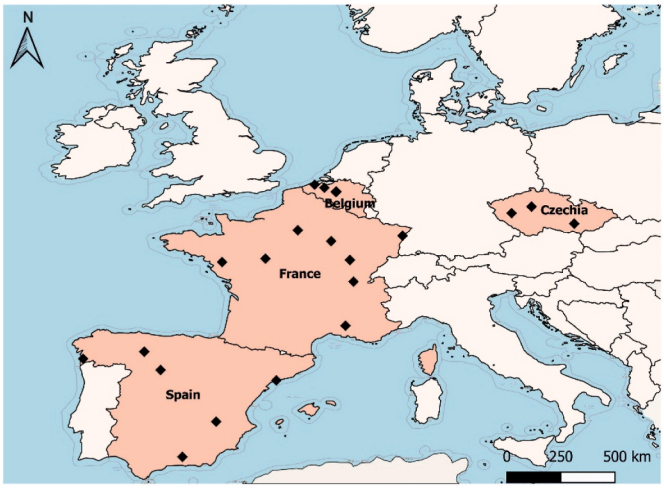

Fig. 2. Location of urban areas from which the building cadastre were collected.

The mean P was finally found to be 60%, with a standard deviation of 18%. By considering $P \geq 60\%$ values as an indicator for building occurrence in each pixel of GHS-BUILT-S2 tiles, a supervised raster classification was carried out to extract the global spatial distribution of building footprints. The classification followed binary logic during which the pixels were classified into zeros and ones, depending on their predefined P values (0: $P < 60\%$; 1: $P \geq 60\%$). The classified raster layers were then joined with the shapefile of worldwide countries.

As during a former step, we executed a zonal analysis again to sum up the values of classified pixels for each country. In this sense, the aggregated country-level values represent the number of cells with buildings in the countries. Finally, the summed numbers were translated to building footprint areas by taking their product with the area of pixels (100 m^2).

The conversion of building footprint to total roof area was depended on the shape and tilt angle of rooftops. Since it is problematic to capture the inter- and intra-regional distribution of these geometric attributes of buildings on global scale, we made certain simplifications. First, it was assumed that all pitched roofs (defined with tilt angle >10°) must be gabled that is one of the most common roof types globally. Based on the study of Byrne et al. (2015), the ratio of flat and tilted roofs was considered to be 25% and 75% for single and multifamily buildings. Besides, the rooftops of commercial and public building types were classified as flat. In addition to these assumptions, we hypothesized that the 75% of single and multifamily rooftops must have such tilt angles that provide the highest solar energy income over the year. The geographical dependence of the optimal tilt angle (β) was calculated with the polynomial equations proposed by Jacobson and Jadhav (2018):

$$\beta_{NORTH} = 1.3793 + \varphi[1.2011 + \varphi(-0.14404 + 0.000080509\varphi)] \tag{2a}$$

$$\beta_{SOUTH} = -0.41657 + \varphi[1.4216 + \varphi(0.024051 + 0.00021828\varphi)] \tag{2b}$$

where φ is the latitude in degrees, β_{NORTH} and β_{SOUTH} is the optimal tilt angle in the Northern and Southern Hemisphere in degrees. Given that most modeling areas have remarkable latitudinal extension, a mean β value was assigned to each region.

The relative occurrence of the building types (f) was determined in the function of roof to floor ratios ($r_{roof\ to\ floor}$; Table S2.) and floor areas (FA) as follows:

$$f_{t,r,p} = r_{roof\ to\ floor_{r,p}} \cdot \frac{FA_{t,r,p}}{\sum_p FA_{t,r}} \tag{3}$$

where t, r and p indices refer to a given year, region and building type,

Fig. 3. Combined GHSL raster and cadastral polygons over Granada, Spain.

respectively. As it is documented in Petrichenko et al. (2019), the BISE transfers the FA values from the 3CSEP-HEB model (Güneralp et al., 2017; Urge-Vorsatz et al., 2012; Chatterjee et al., 2022).

In the light of the building footprint area, f and the mean β values, we calculated the total roof area for each building type and region by considering elementary trigonometry. The total roof area were then reduced to obtain the area that is applicable for installing PV/T collectors. As a reducing term, we employed the so-called utilization factor (U_F; Romero Rodríguez et al., 2017). The U_F is composed of many coefficients to account for area reduction by shadowing (C_{SH}; Kurdgelashvili et al., 2016; Romero Rodríguez et al., 2017), protected areas (C_{PROT}), construction areas (C_{CON}; Byrne et al., 2015), service areas (C_{SA}; Byrne et al., 2015), azimuth (C_{AZ}; Wiginton et al., 2010), slope angle (C_{SL}), panel separation (C_{GCR}; Romero Rodríguez et al., 2017) and occurrence of other solar panels/collectors (C_{PV}/C_{TH}). The majority of the coefficients were predicted based on the related literature (Table S5.). Other coefficients were derived by respecting simplifications for the shape and tilt of rooftops. Considering only a south-facing gable roof, only 50% of the total roof area is suitable for solar panel installation, therefore C_{AZ} was set to 0.5. In our study, C_{SL} expresses the annual influence of using one fixed β for each region on rooftop area availability. Hence, the larger the region, the more significant the overall decreasing effect. It is also important to mention that no protected rooftops were assumed within the projected building stock ($C_{PROT} = 0$). Furthermore, the C_{SH} excludes possible shading from surrounding tall buildings and trees.

In the last step, the available roof area ($RA_{available}$) was calculated in a given year (t), region (r) and for a given building type (p) with the help of the RA and U_F in the following way:

$$RA_{available_{t,r,p}} = RA_{t,\ r,p} \cdot U_{F_{t,r,p}} \tag{4}$$

The RA estimated earlier from the GHSL layer was regarded as an initial value for the first simulation year (RA_{2022}). The temporal dynamics of the RA until 2060 relied on the trends of the FA values of 3CSEP-HEB model (Chatterjee et al., 2022). More precisely, the RA_{2022} was upscaled or downscaled through the growth or shrinking of the FA by:

$$RA_{t,r,p} = \frac{FA_{t,r,p}}{FA_{t-1,r,p}} \cdot RA_{2022,r,p} \tag{5}$$

As Equation (5). indicates, when $FA_{t,r,p} > FA_{t\text{-}1,r,p}$ the $RA_{t,r,p}$ has an increment as compared to the previous year, otherwise the term on the right-hand side is lower than 1. Once $RA_{t,r,p}$ was computed, it was substituted into Equation (4). for each year.

3.4. Technological choice

PV/T systems have been developing continuously in recent years, therefore it was highly important to inspect and specify the most relevant technology-specific modeling variables of PV/T collectors and to update the initial parameters of the previous versions of the BISE. The main goal was to consider the most efficient residential PV/T collectors and apply them on all building rooftops without analyzing the differences of their economic return across the regions.

In order to examine the performance of the state-of-the-art PV/T systems, we reviewed the model specifications of more than 20 PV/T collectors produced or distributed by the largest manufacturers. From the different measures detailed in the data sheets, we focused mainly on the electric and thermal efficiency of PV/T collectors, temperature coefficient for the system's efficiency, inverter's efficiency and nominal power (Table S3.).

Due to the permanent technological innovations, the electric efficiency (η_{elec}) exceeds 20% nowadays, with a maximum of 21–22%. The thermal efficiency (η_{TH}) generally shows higher discrepancies between

Table 1
Technological attributes of PV/T modules used in the analysis.

Variable	Dimensions of PV/T modules
Cell type	monocrystalline Si
Heat exchanger material	copper
P_{max} – ***Nominal power***	375 Wp (DUALSUN, 2021)
$\eta_{r,\ elec}$ – ***Nominal electric efficiency***	21.6% (TRIPLE SOLAR, 2021)
$\eta_{r,\ TH}$ – ***Nominal thermal efficiency***	63.3% (DUALSUN, 2021)
β_p – ***Nominal temperature coefficient***	−0.34%/°C (DUALSUN, 2021)
L_{miscel} – ***Miscellaneous losses***	10%
m – ***Flow rate of fluid***	0.027 (DUALSUN, 2021)

different products, ranging between 60% and 70%. In this study, the reference for η_{elec} and η_{TH} were set being equal to 21.6% and 63.3% (Table 1.). For the temperature coefficient (β_p), determines the dependence of electric efficiency on cell temperature, the lowest (i.e., the optimal) value was found to be around −0.35%/°C. Given that the reviewed PV/T products are characterized by only slight differences (≈0.05%/°C) in β_p, we applied, therefore, −0.35%/°C for this input. Nowadays the efficiency of collectors in converting direct current (DC) to altering current (AC) (η_{INV}) seems to be mostly well above 95%. According to the study of Clean Energy Reviews (2021), the efficiency of the most developed micro inverters can be as high as 98% or slightly above. The η_{INV} is predicted directly by BISE's algorithm (see Section 3.5.), so that the abovementioned values were only taken as references. The peak (or nominal) power (P_{max}) can be converted by the inverter and later transferred to the grid or consumed directly was maximized at 375 W in the current analysis.

All technology-specific variables and their corresponding assumptions used during the modeling activity are summarized in Table 1. We hypothesized a "theoretical" PV/T collector with monocrystalline-Si cells, which currently has the largest market share due to its cost-effectiveness, high efficiency and constantly developing engineering (Gul et al., 2016). This collector was considered to be cell-optimized, integrated with flat plate collector and copper absorber, covered by antireflective tempered glass and uses the mixture of water and glycol as working fluid. It must be noted that two compromises were made due to the modeling design. Firstly, the degradation of solar collectors was disregarded, since the 39-year analysis period is slightly higher than the typical life cycle of PV/T modules. The other simplification, secondly, is related to the future progress of the PV/T technology that is extremely uncertain, therefore the technology-related inputs shown in Table 1 were kept unchanged during the modeling era.

3.5. Computation of solar energy supplied by PV/T collectors

The comprehensive set of algorithms used for calculating the thermal and electric energy generated by the theoretical PV/T system includes some of the methodological aspects applied in other previous studies and in the older version of the model (Homerenergy, 2021; Mainzer et al., 2017; Mangiante et al., 2020; Petrichenko, 2014; Petrichenko et al., 2019). The strength of this particular algorithm is that it requires only easily obtainable and reproducible input data for meteorological and technological measures. The most important steps of the implemented calculation process of the BISE model are presented in the Supplementary Material.

4. Results and verification

In this section, we focus on presenting the spatiotemporal changes in the technical potential of the simulated solar electric and thermal energy supplied by PV/T collectors across regions and on the rooftops of different building types. For better understanding the expected trends of the PV/T potential, we found important to show the outcomes of GIS-based estimations carried out for the variation of building rooftop area availability during the modeling period. Albeit the model has very fine spatial resolution, we generally preferred to aggregate the data for regions and yearly time step for an easier interpretation. However, to have a more insight on the daily and inter-seasonal characteristics of solar energy production, results at hourly and monthly temporal resolution are also presented. In the following, the total PV/T energy output is divided by energy forms and so the results for the thermal and electric energy supply are shown separately to better investigate the areal differences in the solar energy utilization of rooftop PV/T collectors.

4.1. Estimated changes of building rooftop area availability

The estimated regional total rooftop area values vary between 3 and 70 billion m^2 in the first year of the simulation period (Fig. 4.). In other words, there is a difference of about 23 times in thus factor between the CPA and EEU regions, typified with the largest and smallest RA dimensions. By contrasting the proportion of the calculated total roof areas to the total land area of the regions, informative regional urbanization levels can be quantified. This ratio, for example, is 60‰ and 38‰ in the CPA and PAS regions, while it remains only around 3‰ and 10‰ in the AFR and FSU regions. This implies that the building coverage and thus the degree of urbanization were found to be much higher in the former regions than in the latter ones. Practically it means that in regions with more intense urbanization, there are larger energy needs (due to higher and more concentrated population density) and more favorable infrastructure potential (e.g., more developed grid system or higher accessibility to the grid) for efficiently harnessing the available solar energy on rooftops rather than occupying multifunctional land resources.

Since the BISE model (via the 3CSEP-HEB model) estimates an extending building stock (i.e., ongoing urbanization) towards 2060 across the regions, it is manifested in an increasing trend in the total RA during the modeling period (Fig. 4.). A fundamental rule-of-thumb of this growth is that the dynamics are usually lower in the regions, where the predicted RA_{2022} values are initially higher (e.g., NAM, CPA and WEU). For instance, the annual growth in the WEU region was predicted to be around 0.25 billion m^2/year, while this value exceeds 1.2 billion m^2/year for the LAC region. Similarly high RA increases are observable in the MEA and PAS for which mean annual growths of 1–1.1 billion m^2/year were found. As a consequence of the outlined trends, the CPA, LAC and NAM regions are characterized with the RA maxima by the end of the modeling period, with related values of 122, 62 and 46 billion m^2, respectively.

For estimating the solar technical potential on building rooftops, the available roof area ($RA_{available}$) is of much more importance than the RA. Based on Equation (4)., the $RA_{available}$ is calculated by multiplying the RA with the U_F. Given that values between 28 and 31% were assumed for the U_F (Table 2.), approximately one third of the total RA was considered to be suitable for the installation of PV/T collectors during the modeling activity. The heterogeneous values of the U_F summarized in Table 2 are influenced, in foremost, by the shares of the different building types. Secondly, their heterogeneity stems from the tilt and shading factors, more pronouncedly in the higher latitudes. As the ratio of commercial/public buildings with more frequent flat roofs is expected

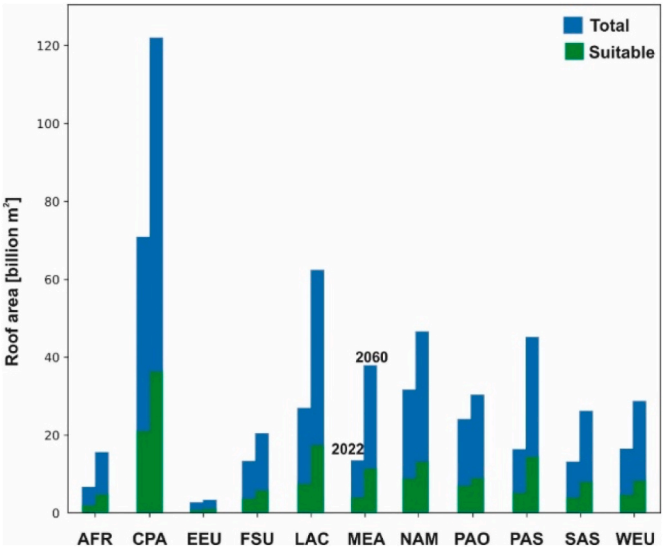

Fig. 4. Estimated total roof area and suitable building rooftop area [in billion m^2] for solar panel's installation by regions in 2022 (columns on the lefts) and 2060 (columns on the rights).

Table 2
Estimated regional values of utilization factor in the starting and ending year of the modeling period.

Region	U_{F_2022}	U_{F_2060}
AFR (Sub Saharan Africa)	0.29	0.25
CPA (Centrally Planned Asia)	0.28	0.28
EEU (Central and Eastern Europe)	0.31	0.31
FSU (Former Soviet Union)	0.28	0.28
LAC (Latin America)	0.26	0.26
MEA (North Africa and Middle East)	0.28	0.28
NAM (North America)	0.28	0.28
PAO (Pacific OECD countries)	0.29	0.28
PAS (Other Pacific Asia)	0.30	0.30
SAS (South Asia)	0.28	0.25
WEU (Western Europe)	0.28	0.28

to increase in most regions (will be discussed later; Table S6.), therefore a small decrease in the U_F can be anticipated (especially for low latitudes due to high C_{GCR}) by the end of the simulation period (Table 2.). In another interpretation, the solar installation potential per 1 m^2 may be slightly lower by 2060, due to the changing structure of building stock.

Due to the presented U_{F_2060} values and the explicit connection between the RA and $RA_{available}$, the highest installable rooftop area can be expected by 2060 in the CPA, LAC and PAS regions (36, 17 and 14 billion m^2, respectively) (Fig. 4.). In the meantime, the lowest $RA_{available}$ were projected for the AFR (4.75 billion m^2) and EEU (1.2 billion m^2). In relative sense, the CPA, LAC and PAS have the contributions of 28%, 13% to the aggregated global $RA_{available}$, respectively. Regions with the 4 smallest areas, on the other hand, are expected to account for only 15% of the global value.

4.2. Estimated changes of technical potential for solar electric and thermal energy production

In addition to the $RA_{available}$, the geographic exposure of solar collectors is also a crucial component in determining the technical potential of rooftop PV/T energy production, as underlined by the modeled energy output supplied per 1 m^2 of solar collectors ($E_{EL\ output}$ and $E_{TH\ output}$) (Fig. 5.). The $E_{TH\ output}$, generally, is the most significant in regions with large fraction of areas around the Subtropics, where the geographical potential of solar energy is the highest on the Earth. The regions with substantial $E_{TH\ output}$ include the PAO (544 kWh/m^2), SAS (541 kWh/m^2), LAC (501 kWh/m^2) and MEA (497 kWh/m^2). The potential for $E_{EL\ output}$ depicts slightly different spatial patterns than that of for the $E_{TH\ output}$. The highest potentials of PV/T collectors for electricity production

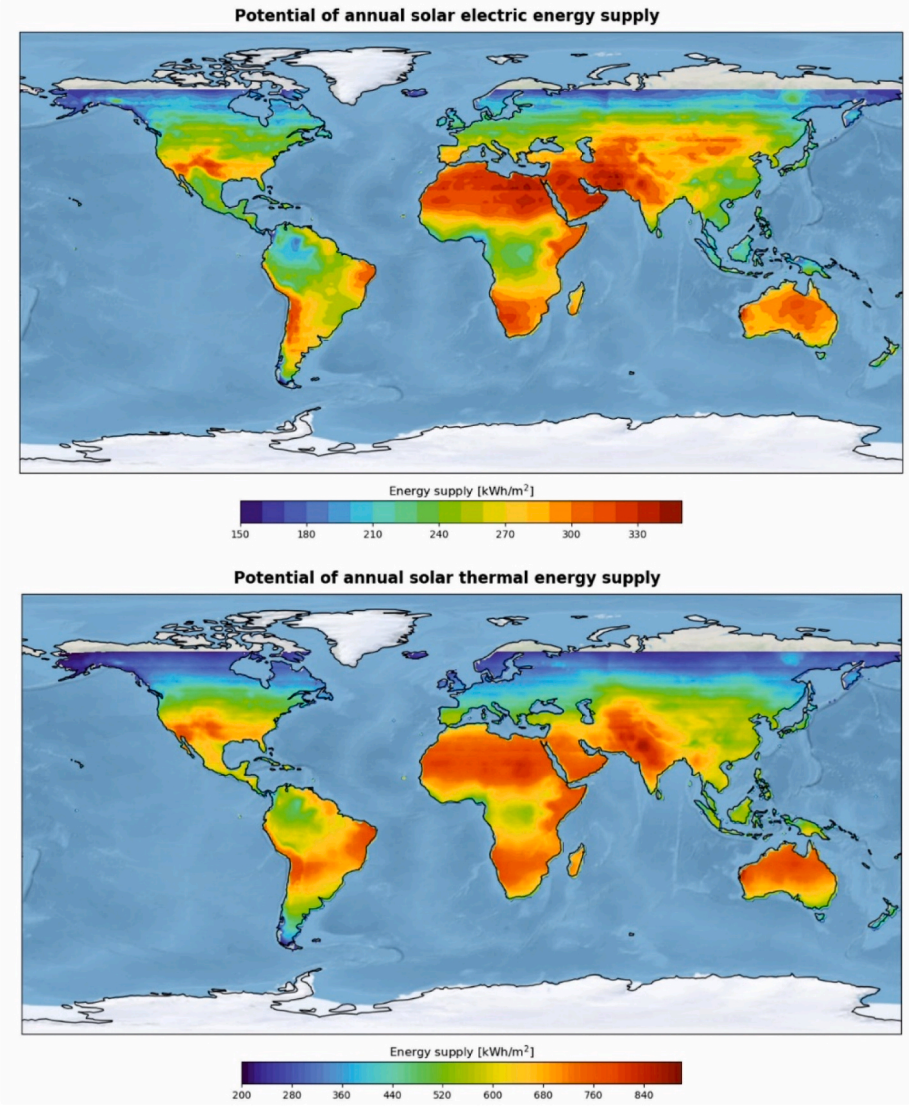

Fig. 5. Mean potential of PV/T energy production (for electric energy on the top, for the thermal energy on the bottom; in kWh/m^2) on 1 m^2 of the available building rooftop area. Due to data lacking, values for latitudes beyond 66.5° were not illustrated.

were determined for the MEA (294 kWh/m^2), PAO (286 kWh/m^2) and SAS (267 kWh/m^2). Comparing the inter-regional electric and thermal potentials, the largest gap between the $E_{EL\ output}$ and $E_{EL\ output}$ occurs in the LAC and PAO (i.e. more favorable circumstances for supplying thermal energy), which is related to $E_{EL\ output}$ the high frequency of the (warm) climate zones within the region and hence to the frequent episodes with overheated PV/T cells.

Based on the results shown in Fig. 5., the SAS (715–1215 kWh/m^2), PAO (525–1215 kWh/m^2) and MEA (810–1170 kWh/m^2) regions can be characterized by the highest combined PV/T potential for electricity and thermal production. However, there are also many "hotspots" in other regions (e.g., Southeastern part of the USA in the NAM or Southeast Africa in the AFR) where the total rooftop PV/T potential may be substantially large (i.e., above 1000 kWh/m^2).

Due to the outlined characteristics for roof parameters and geographical potentials at Figs. 4 and 5., the technical potential of solar electricity supply ($E_{EL\ total\ supp}$) was modeled to be in a range between 0.2 and 5.5 PWh in 2022. By comparing Fig. 4 and Table 3., the strong dependence between the $RA_{available}$ and the $E_{EL\ total\ supp}$ magnitudes can easily be identified. It results in that the technical potential is characterized by its regional maxima in the CPA, NAM and LAC for the beginning of the modeling era.

As it was emphasized earlier, the (solar) climate of different geographical areas, additionally to the $RA_{available}$, is considered as an important component in driving the technical potential of PV/T energy production, although this factor may have lower importance as compared to the $RA_{available}$. To shed a little more light on this sensitivity, the difference in the $RA_{available}$ between the AFR and CPA is used as a reference, which was estimated to be about twelvefold for the base year of 2022. Meanwhile, the difference in the $E_{EL\ total\ supp}$ is only tenfold, meaning that the higher average annual radiation income received by the AFR (and other) region(s) can slightly compensate the sparser roof area availability via the substantial $E_{TH\ output}$.

Nevertheless, due to the primary relevance of the $RA_{available}$ and the related variations depicted in Section 4.1., the most noticeable changes in the $E_{EL\ total\ supp}$ can be expected in the developing regions (e.g., LAC, PAS and MEA) between 2022 and 2060. On annual basis, these changes were predicted to be 90 TWh/year in the LAC, 60 TWh/year in the MEA and 50 TWh/year in the PAS. As a result, the $E_{EL\ total\ supp}$ could remain relatively inhomogeneous among the regions by 2060, reaching their maxima in the CPA, NAM and LAC, with 9.7, 6.0 and 4.5 PWh, respectively (Table 3.). The most restrained potentials, on the other hand, are expected in the EEU (0.24 PWh) and AFR (1.28 PWh) where either the geographical (climatic) or the utilization potential of solar collectors may be reduced.

Since the differences in PV/T solar energy supply between regions and the subsequent temporal changes during the simulation period are shaped chiefly by the $RA_{available}$, similarly to the $E_{EL\ total\ supp}$, the highest $E_{TH\ total\ supp}$ is also seen in the CPA (9.5 PWh) for 2022. Though the projected $RA_{available}$ is lower in the PAO in contrast with the NAM region, the thermal output was found to be about 50% higher in the earlier region (PAO: 3.8–3.9 PWh and NAM: 2.6 PWh). This is related to the geographical exposure of the NAM that has subpolar territories (e.g., Alaska), where the annual magnitude of $I_{TOT,\ tilt}$ and thus convertible solar energy is limited throughout the year.

As the inter-annual variability of $I_{TOT,\ tilt}$ was estimated to be insignificant over the analyzed years, the yearly dynamics of $E_{TH\ total\ supp}$ are almost exclusively influenced by the $RA_{available}$. As a result, the largest increases are seen again in the CPA (180 TWh/year), LAC (120 TWh/year) and PAS (110 TWh/year) regions, while the smallest annual changes were modeled for the EEU (1.2 TWh/year) and FSU (13 TWh/year), being well below the predicted mean global growth of 70 TWh/year. Due to outlined tendencies, the technical potential of rooftop $E_{TH\ total\ supp}$ could expand to be between 0.28 (EEU) and 16.5 PWh (CPA) by 2060 (Table 3.).

Table 3 highlights that, as a direct consequence of the more efficient conversion of irradiance into thermal energy (i.e., higher η_{TH} than η_{elec}), the technical potential of solar thermal energy production is about the double that of electricity production in most regions. Also, the $E_{TH\ total\ supp}$ seems to be much more sensitive to the $I_{TOT,\ tilt}$ than the $E_{EL\ output}$. This can be underlined by the comparison of $E_{EL\ total\ supp}$ and $E_{TH\ total\ supp}$ in climatic point of view. The difference between these two types of energy outputs is twofold for regions with lower latitudes and abundant radiation ($I_{TOT,\ tilt} > 2000$ kWh/m^2) (e.g., the PAS, SAS and MEA), while this gap is reduced to only 5–10% in the FSU or EEU ($I_{TOT,\ tilt} < 1500$ kWh/m^2 and low T_C variability). In fact, this phenomenon can be explained with the thermal attribute of silicon cells. When $I_{TOT,\ tilt}$ is high (in areas with warm and dry climate), the solar cells are exposed to enhanced radiation income and more frequent episodes of high T_c related to collectors being located under cooler and moister climate. In the first case, consequently, the electric efficiency of the system drops but an increased amount of heat is absorbed by the transfer fluid of the PV/T collector. In the second case, however, the T_c is usually lower, hence the electric efficiency remains relatively high and less thermal heat is channeled into the system.

Table 3
Annual technical potential of modeled solar electric and thermal energy production [in PWh] of PV/T collectors by regions for 2022 and 2060.

Region	Electric		Thermal	
	2022	2060	2022	2060
AFR (Sub Saharan Africa)	0.56	1.28	0.91	2.11
CPA (Centrally Planned Asia)	5.52	9.73	9.48	16.51
EEU (Central and Eastern Europe)	0.20	0.24	0.24	0.28
FSU (Former Soviet Union)	0.92	1.40	0.90	1.39
LAC (Latin America)	1.95	4.50	3.77	8.76
MEA (North Africa and Middle East)	1.20	3.40	2.02	3.80
NAM (North America)	2.31	6.00	2.61	6.73
PAO (Pacific OECD countries)	2.03	2.53	3.85	4.83
PAS (Other Pacific Asia)	1.19	3.30	2.34	6.51
SAS (South Asia)	1.07	2.19	2.14	4.38
WEU (Western Europe)	1.09	1.91	1.22	2.13
TOTAL	**18.04**	**36.48**	**29.48**	**57.43**

4.3. Estimated shares of technical potential for solar energy supply between building types

In order to explore how the $E_{PV/T\ total\ supp}$ (i.e., the sum of $E_{EL\ total\ supp}$ and $E_{TH\ total\ supp}$) is distributed among building types, their regional values were disaggregated by employing the respective regional shares of $RA_{available}$ (Table S6.). Of the seven analyzed building subcategories, single family buildings were projected to account for about 50% of the global technical potential of $E_{PV/T\ total\ supp}$ (24.8 PWh) in the first year of the investigation period (Fig. 6.). The share of multifamily and commercial/public buildings in the $E_{PV/T\ total\ supp}$ is predicted to be 31% (13.5 PWh) and 19% (9.3 PWh). The maxima of the modeled $E_{PV/T\ total\ supp}$ at single family buildings, due to their high absolute and relative $RA_{available}$ values, occur in the CPA (8.2 PWh) and NAM (3 PWh). For similar reasons, the dominance of the CPA region is also observed for the other residential and the tertiary building types, too (multifamily: 3.5 PWh and commercial/public: 3.4 PWh). As a result of the second largest suitable rooftop space in the PAO for multifamily buildings, the highest local production was predicted for this class by 2.3 PWh. For commercial/public buildings, the simulated potentials are nearly homogeneous spatially after the CPA, indicated by having $E_{PV/T\ total\ supp}$ around 2 PWh in several regions (LAC: 2.3; PAO: 1.8; NAM: 1.5 PWh).

Although Table 3 suggests that the aggregated $E_{EL\ total\ supp}$ and $E_{TH\ total\ supp}$ are characterized by year-to-year increases, $E_{PV/T\ total\ supp}$ shows decrease within several regions for some building types over the simulation period (Fig. 6.). This negative trend generated by the decreasing share of a given building type is specifically tied to single family and multifamily buildings. For single family buildings, in fact, two separate

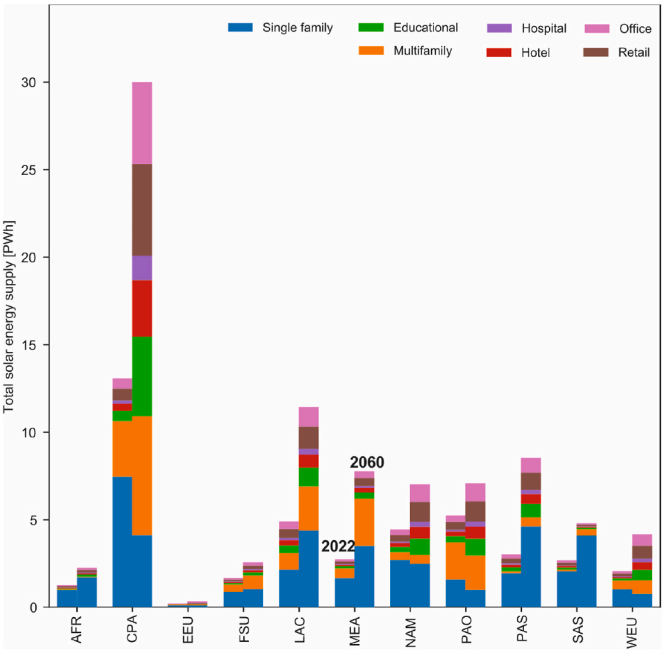

Fig. 6. Estimated annual PV/T technical potential of solar energy production [in PWh] by regions and building types for 2022 (columns on the left) and 2060 (columns on the right).

trends are noticeable. For developed regions (e.g., NAM, PAO, WEU and EEU) and for the CPA, the technical potential may slightly decrease by time, while for developing regions (e.g., LAC, PAS and SAS), an opposite trend was predicted, due to the (faster) expansion of the associated building stock. The share of technical potential at multifamily buildings shows shrinking exclusively in the PAO region. These changes for the shares of residential buildings are strongly connected to building stock estimations implemented from the HEB model (Chatterjee et al., 2022) (Table S6.).

By 2060, the $E_{PV/T\ total\ supp}$ was estimated to have the following distribution between the building types: single family buildings: 31.5 PWh (31%), multifamily buildings 18.7 PWh (21%) and commercial/public buildings 39.8 PWh (44%) (Fig. 6.). This suggests that the (faster) growth in the number of commercial/public buildings leads to an increase in the associated $RA_{available}$, which, in some regions (e.g., CPA, WEU and PAO), results in larger $RA_{available}$ (and technical potential) as compared to residential buildings. Within the tertiary category, the "offices" and "retails" appear to be the most favorable in terms of solar energy generation by 2060. The contribution of "offices" to $E_{PV/T\ total\ supp}$ was projected to vary between 1 and 15% of the total building stock.

For having an even more complete picture on the ability of a given building type in generating solar energy on rooftops, we took also the vertical characteristics of the buildings (e.g., number of floors or height) into consideration and have calculated the solar production per 1 m^2 of floor area of the building ($E_{PV/T\ total\ supp}$*). Note that this parameter depends significantly on the region and building type dependent $r_{roof\ to\ floor}$ (Table S4.) and can be a well interpretable measure in energy supply-demand comparison. Due to the limited vertical extension (i.e., low number of stories), the $E_{PV/T\ total\ supp}$* was estimated to be the largest for single family and (commercial/public) retail buildings, with around 119.7–642 and 92.8–746.7 kWh/m^2 (Fig. 7.). Multifamily and (commercial/public) office buildings estimated to be with 7–11 stories on average, can be found on the other side of the spectrum (MF: 11.2–299.3 kWh/m^2; C&P Offices: 5.2–210.9 kWh/m^2). Consequently, unlike at high-rise buildings, the application of PV/T collectors on horizontal surfaces of low-rise tertiary buildings has always the highest potential, regardless of the analyzed region. Presumably, this dichotomy may have a reverse impact on the ability of these building classes in balancing the local consumption with the energy generation of rooftop PV/T systems.

4.4. Temporal variation of PV/T solar electric energy supply across regions

Because of the geographical dependence and substantial temporal variability of solar radiation, there are very diverse intra-annual profiles of the technical potential of PV/T energy production across the regions. It can be concluded that the simulated shapes of the representative curves for the $E_{TH\ output}$ and $E_{EL\ output}$ are in a robust connection with the annual magnitudes of the solar irradiation (Fig. 8.), as it was partly discussed at Fig. 5. Analyzing first the annual variability of the $E_{TH\ output}$, the highest peaks are outlined in the SAS (146.7 kWh/m^2) and PAO (156.9 kWh/m^2) regions. The simulated $E_{TH\ output}$ curves, except for the MEA and SAS regions, show two maxima over the typical year. In the AFR and PAS, for example, the highest $E_{TH\ output}$ can be observed during the solar equinoxes (end of March and September). In the LAC and PAO, on the other hand, outstanding values were estimated to be rather in late December/early January. In the mid-latitude regions (e.g., NAM, WEU and EEU), the maximum occurs in May and September, as thick convective (cumulonimbus) clouds dampen the irradiance frequently during the summer months. Presumably, the opposite reason could have led to the balanced (single-peaked) summertime maximum in the MEA. In the SAS, the single peak in spring can be explained by the long-lasting monsoon period. In summary, the regional differences in the inter-annual variability of $E_{TH\ output}$ seem to be proportional to the number of seasons. Hence, considerable variability is outlined for the CPA (96.6

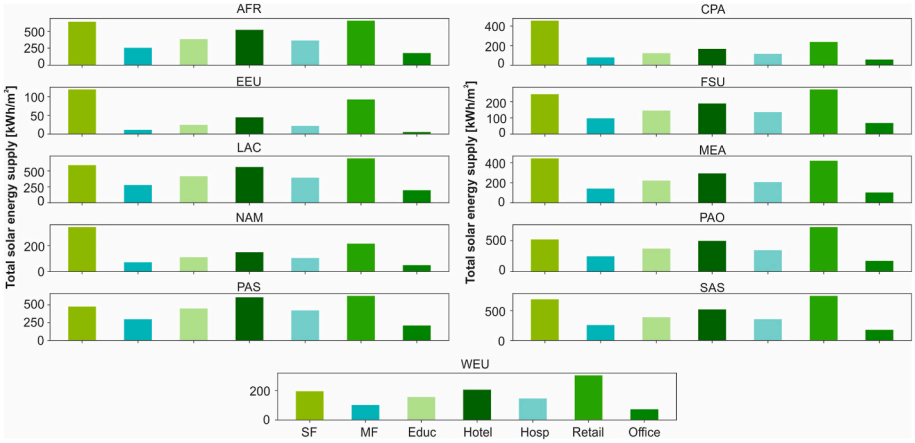

Fig. 7. Estimated PV/T technical potential of solar energy production [in kWh/m^2] by regions and building types for 1 m^2 of the floor area in 2022.

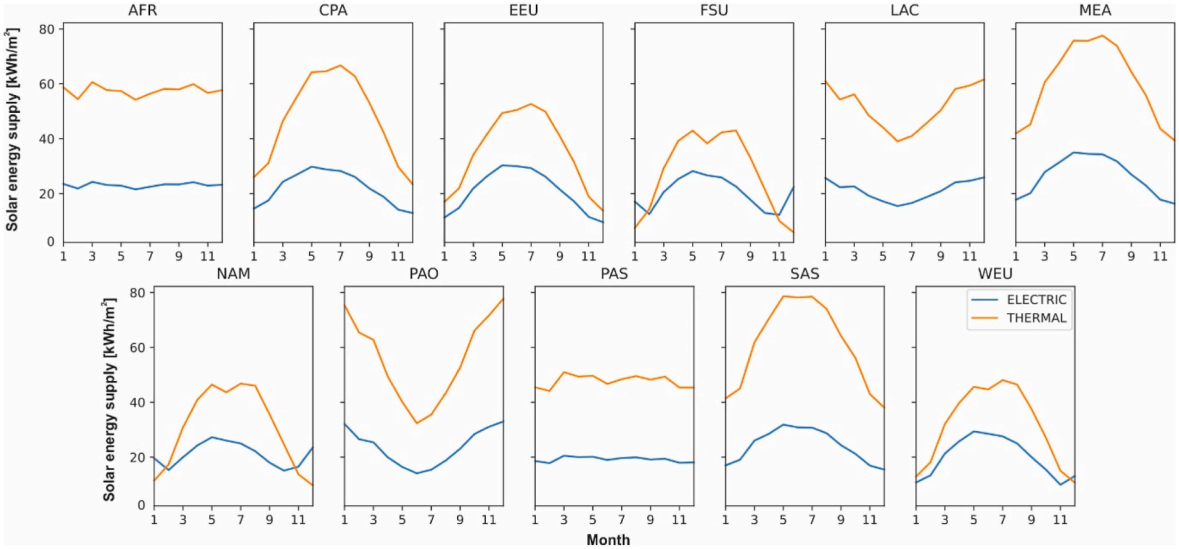

Fig. 8. Estimated mean monthly variability of technical potential of solar electric (blue curves) and thermal (red curves) energy production [in kWh/m^2] by regions over the analyzed period.

kWh/m^2) and NAM (91.8 kWh/m^2), while the lowest fluctuations were simulated for the PAS ($\Delta E_{TH\ output}$: 15.9 kWh/m^2) and AFR (13.3 kWh/m^2).

The temporal peaks (FSU: 78.6 and NAM: 77.3 kWh/m^2) and annual fluctuations (6.7–59.2 kWh/m^2) of the $E_{EL\ output}$ were estimated to be lower related to the $E_{TH\ output}$ (Fig. 8.). It is also a noticeable characteristic, as already pointed out in Section 4.2., that the difference between the two types of energy productions could be smallest in the FSU, NAM, EEU and WEU. On the top of that, during cold winter days without cloud coverage and snowfall, the $E_{EL\ output}$ was simulated to overcome the $E_{TH\ output}$ in these regions.

Since the inter-regional profiles of the $E_{TH\ output}$ and $E_{EL\ output}$ are highly varying over a shorter frequency than a year (especially at mid-latitudes), it is relevant to inspect the corresponding profiles on daily basis. To do so, we selected two climatically and astronomically important days (e.g., winter solstice – 12. 21. and summer solstice – 06. 21.) of a randomly picked year (Fig. 9a. and 9b.). In general, the modeled daily profiles are described by spreading bell-shaped curves, with a peak around the local noon and with a rising (falling) phase in the morning (afternoon). Moreover, the daily dynamics of the $E_{TH\ output}$ are undoubtedly much more intense related to that of the $E_{EL\ output}$, which is manifested in a rapid uptake (declining) period in the morning (afternoon). The summer solstice day illustrates that, although there is winter in several regions on that day (parts of predominantly South Hemispheric regions; e.g., LAC or AFR), the magnitude of $E_{TH\ output}$ can still be about the same or slightly higher in the LAC and AFR as compared to the respective values in the EEU or in the FSU (Fig. 9a.). The $E_{EL\ output}$, however, has always higher values in areas with real summer conditions. Being in line with monthly profiles, the electricity output is of a ususal indominance over the thermal yield, with an exception around in the beggining of and at the end of the daytime.

Whilst the $E_{EL\ output}$ was estimated to be higher than $E_{TH\ output}$ only around sunset and sunrise on 21st June, this was found to come about during most of the daytime hours on 21st December in the WEU, EEU, FSU and NAM regions. This “crossover”, caused by low sun elevation and irradiance, is restricted to the middle and high latitudes, so that the

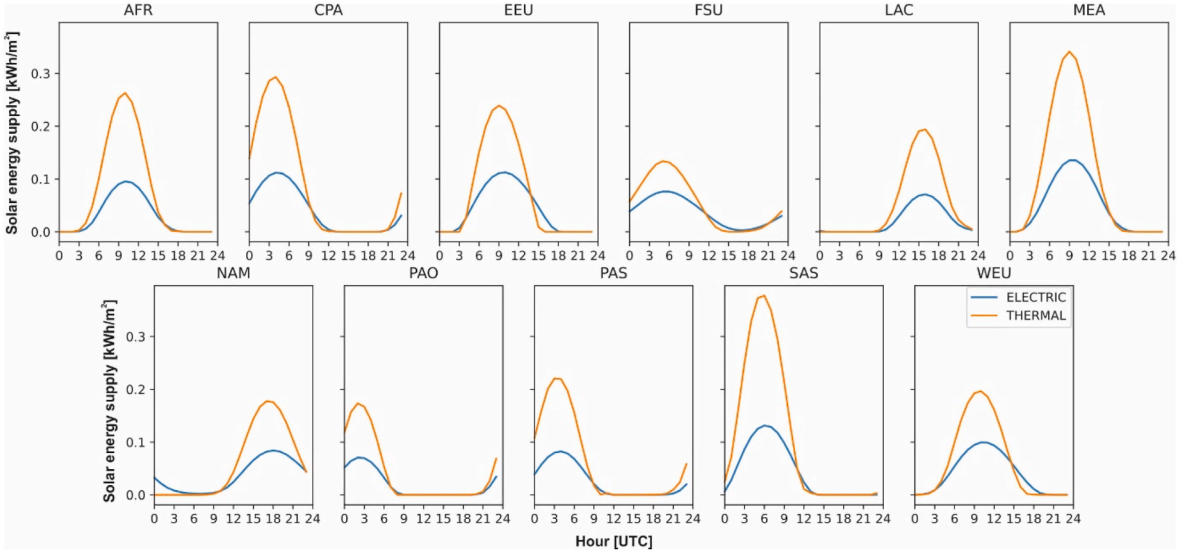

Fig. 9a. Estimated mean hourly variability [in UTC] of technical potential for solar electric (blue curves) and thermal (red curves) energy production [in kWh/m^2] by regions during the summer solstice.

$E_{TH\ output}$ was simulated to be still higher during the winter solstice at the lower latitudes. It is known that as the solar altitude decreases, the path travelled by sunlight and the ratio of diffuse to direct radiation are increased. Therefore, Fig. 9a and 9b can be interpreted as that where the proportion of direct radiation is higher on a given day (e.g., AFR, PAO, LAC), the T_C of the PV/T collector is elevated, hence more waste thermal energy (more $E_{TH\ output}$) is being generated. On the other hand, where the radiation is more scattered and attenuated (i.e., higher latitudes and winter months), the magnitude of $E_{TH\ output}$ is smaller, although this amount of radiation is still suitable for being converted to electric energy.

Nonetheless, it is important to note that the model does not take the snow, leaf or mud coverage of PV/T collectors into account, so that the real wintertime $E_{TH\ total\ supp}$ and $E_{EL\ total\ supp}$ in cold areas may be lower than the simulated values. Moreover, due to the large longitudinal and latitudinal extension of the regions and the significant variability of the solar irradiance, the respective diurnal profiles in some sub-regions might be different due to site-specific environmental conditions.

4.5. Model verification

4.5.1. Total and available roof area

According to our analysis, the total roof was estimated to be about 220 billion m^2 and around its one third can be suitable for solar energy harness with PV/T collectors. In general, the roof area availability was found to be largest in the most urbanized areas (e.g., CPA and NAM) where the building stock is well extended. The dynamics of the (total and available) roof area were relied on the reference roof area data (i.e., the one derived from geospatial sources) as well as regional population (UN, 2018), GDP (OECD, 2021) and specific floor area (in m^2/person or m^2/$) estimations from the 3CSEP-HEB model (Chatterjee et al., 2022). Since the projection of these socio-economic parameters has its methodological limitations, the estimated shares of residential and tertiary rooftops include certain uncertainties.

Although the validation of our results for the total and available roof area cannot be complete (e.g., very different regions of interest), the related magnitudes seem to be in line with other references from the literature. For the European Union, for instance, Bódis et al. (2019) found the $RA_{available}$ to be around 7935 million m^2. This value is slightly larger than that of the sum in the BISE for the WEU and EEU regions (5632 million m^2). Because of the similarities of the methodologies, this could be the consequence of the different threshold value applied for the building raster layers. By using finer resolution LIDAR data for the US, Margolis et al. (2017) estimated a useful area on the rooftops to be 4922 million m^2. Although the North American region also includes Canada in the BISE, the $RA_{available}$ was projected to be 4795 m^2 in our analysis, indicating also some underestimation. For China, on the other hand, we found a larger value as compared to that published in the study of Grau et al. (2012). Therefore, no clear tendency of over- and underestimation is outlined based on this inherently constrained comparison.

4.5.2. Technical potential of rooftop solar energy production

Since there are no estimations of PV/T energy production on global scale to best of the authors' knowledge, we can only validate the modeled $E_{EL\ total\ supp}$ values against the results of global and regional studies designed for quantifying the technical potential of rooftop PV panels. As Table 4 indicates, the simulated technical potentials of the corresponding electricity generation in the reviewed investigations

Table 4
Comparison literature estimations of the technical potential of solar electric energy supply.

Study	Region	Temporal validity (other ↔ current study)	Estimation by cited study [PWh]	Estimation by previous BISE [PWh]	Estimation by upgraded BISE [PWh]
Hofman et al. (2002)	Global	2020 ↔	7.70	5.16	18.04
	AFR	2022	0.66	0.60	0.56
	LAC		0.78	0.40	1.95
	MEA		0.57	0.22	1.20
Hoogwijk (2004)	Global	2004 ↔	6.00	7.20	18.04
	EEU	2022	0.10	0.08	0.20
	MEA		0.30	0.22	1.20
	FSU		0.20	0.18	0.92
	NAM		1.10	0.80	2.31
	WEU		1.10	0.42	1.09
Joshi et al. (2021)	Global	2020 ↔	27.51	7.20	18.04
	EEU	2022	0.65	0.08	0.20
	LAC		0.80	0.40	1.95
	MEA		0.46	0.22	1.20
	NAM		4.75	0.80	2.31
	WEU		2.21	0.42	1.09
Bódis et al. (2019)	WEU	2016 ↔	0.54	0.42	1.09
	EEU	2022	0.14	0.08	0.20

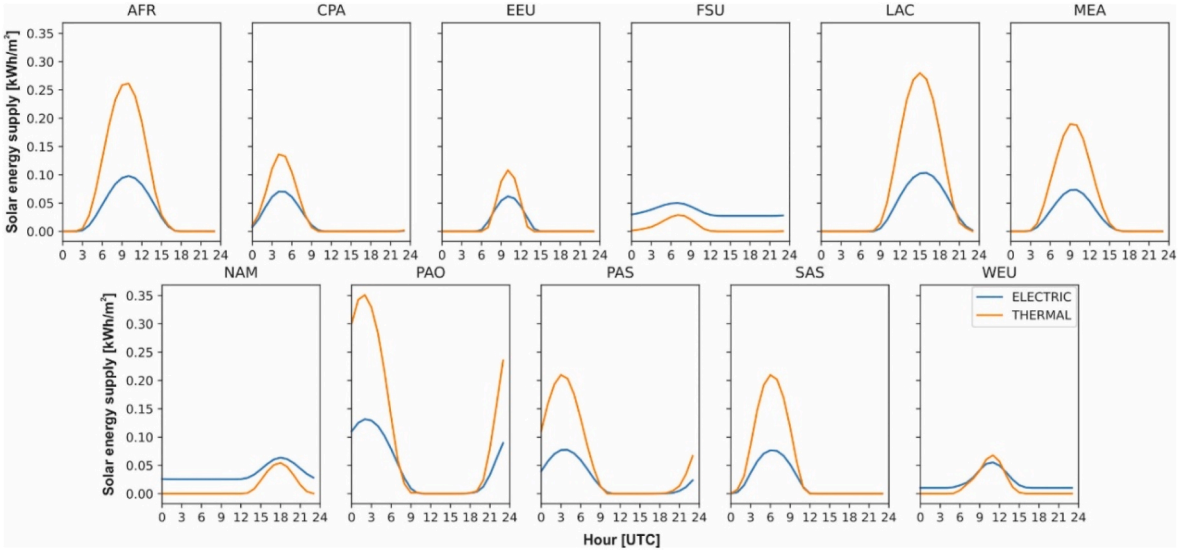

Fig. 9b. Estimated mean hourly variability [in UTC] of technical potential for solar electric (blue curves) and thermal (red curves) energy production [in kWh/m^2] by regions during the winter solstice.

seem to be fairly diverse, having a range between 6 (Hoogwijk (2004) to 27.51 PWh (Joshi et al., 2021). Therefore, the 18.04 PWh of electric output given by the upgraded BISE model is in the upper end of this scale.

The differences among the results are presumably related to the dissimilar target periods, rooftop area approaches and technological measures. Since the technology of the solar panels has improved drastically in the recent years, the earlier studies projected the lowest energy supply, due to the lower electric efficiencies and nominal powers of their hypothesized system. In Hoogwijk (2004), for example, the η_{EL} was set to 14%, which has been remarkably exceeded over the years by the current state-of-the-art PV panels. Another explanation for the lower $E_{EL\ total\ supp}$ values in Hofman et al. (2002) and Hoogwijk (2004) may stem from the preference of less accurate empirical (or statistical) assumptions for the RA_{total} in contrast with more reliable GIS-based methods. On the other hand, it is a common feature of the reviewed modelling assessments that they all calculated the largest technical potentials for the North American (e.g., USA), East Asian (e.g., China) and European (e.g., Germany) countries.

If the simulation of the upgraded BISE model and the one of the most recent global study (Joshi et al., 2021) is compared, it can be concluded that they predicted around 9.5 PWh larger values for the $E_{EL\ total\ supp}$ than that of in our analysis (Table 4.). This 52% difference, however, is attributed to that Joshi et al. (2021) hypothesized the U_F to be 1 (all rooftop area is covered with solar systems), while we considered values between 0.28 and 0.33 for this variable. Nevertheless, they offset the high $RA_{available}$ with very low η_{EL} (Joshi et al., 2021: 10%; this study: 21.6%). Despite the different GIS approach employed in their analysis for deriving building geometry (i.e., machine learning method based on road length, population, built-up area boundaries and building footprint), the estimated RA_{total} values indicate a great agreement (Joshi et al., 2021: 193 875 km^2; this study: 217 187 km^2). It underlines, therefore, the essence of the choice of the U_F in shaping the final result for the $E_{EL\ total\ supp}$.

Similar conclusion can be drawn based on the comparison of the estimations produced by the previous and the upgraded version of the BISE model. Table 4 shows that there is about a threefold difference in the $E_{EL\ total\ supp}$ between this analysis and the one presented in Petrichenko et al. (2019). Being the results of the outdated BISE in the same cluster as Hofman et al. (2002) and Hoogwijk (2004), it is assumed that our latest results could better capture the current rooftop potential for solar energy production as a consequence of the fine-tuned input data for rooftop geometry, meteorology and technology. Regionally, certain uncertainties may persist in the new methodology. For example, such bias is observable for the African region where the magnitude of the $E_{EL\ total\ supp}$ remained in the same extent in spite of the more developed solar collector's metrics assumed in this study.

5. Discussion

This study demonstrated the future technical potential of building rooftop energy production of PV/T collectors by using the BISE model at global and regional scale. The modeling of building-integrated solar energy production is a crucial step to understand the feasibility of net-zero buildings that can play a vital role in decarbonizing the entire building sector across the world. This modeling task involved several challenges, including data collection, synthetization and optimization for the purposes. One of the key was to derive the cardinal inputs for total and suitable roof area. In doing so, the main priority was to produce this data with the same input and methodology for all regions.

As the building coverage represented by the GHSL pixels can be spatially very diverse, the number of building cadastre invoked to determine the probability of occurrence of buildings (P) has a crucial role in the retrieval of the final P. Although we tried to maximize the number of polygons (close to 6 million) from urban areas with different size and structure, we presumably underestimated the potential location of building footprints and obtained varying accuracy across the regions. The accuracy was also influenced by the resolution of the raster layers (i.e., 10 m), which inherently filtered the smallest buildings out from the analysis. Many studies have used alternative, remotely sensed data (e.g., LIDAR; Brito et al., 2012; Margolis et al., 2017) to extract building footprints, however, it is easily considerable that this method would not be fully applicable to the global distribution of the entire roof surface. Another alternative for that would have been, with major areal simplifications, the automated detection of buildings with the help of easily accessible datasets (e.g., Google Street View; Kang et al., 2018).

In the estimation of the U_F, the greatest challenge was to give a proper approximation on the tilt angle of the roofs. As the BISE model was developed to determine the maximum technical potential of solar energy generation, estimating the slope of roofs with only one ideal angle may be a relevant assumption. However, due to the subdivision of the regions and the construction of the methodology (see Equation (4).), only one average tilt value was assigned to each region, which could vanish the regional variations of roof geometry due to the large north-south extension of the regions. Despite the methodological limitations, overall, the values found for the U_F (around 0.3; see Table 2.) are in line with those found in the literature: from 0.2 (e.g., Lopez et al., 2012) to 0.55 (e.g., Peng and Lu, 2013).

Beyond the approximation for the RA and $RA_{available}$, the uncertainties of the technical potential of $E_{PV/T\ total\ supp}$ might also be related to other factors. However, it was predicted in some studies (e.g., Deng et al., 2015) that the potential for electricity generation of solar panels on the rooftops could be doubled between 2030 and 2070 globally, the progress of the PV/T technology and the availability of materials for fabrication are fairly unknown. In the BISE, the expected growth of the efficiency of PV/T collectors was taken out of consideration, which was slightly adjusted by neglecting the degradation of solar systems (ranging typically between 0.5 and 1% per year; Jordan and Kurtz, 2013). In spatial term, the occurrence of the simulated tendencies in the future depends mostly on how fast the developing countries become interested in phasing out fossil energy and on how they can promote the solar energy despite the fear of consumers from the long payback period of installing solar systems (Shukla et al., 2017).

Even with the abovementioned limitations and owing to the conservative modeling approach, the BISE simulated a global $E_{PV/T\ total\ supp}$ of 47.6 PWh by 2022, which means a substantial potential of building integrated solar production. To this summed value, the contribution of $E_{EL\ total\ supp}$ and $E_{TH\ total\ supp}$ was estimated to be 29.5 (62%) and 18.1 PWh (38%). Remarkable potential can be deployed by countries in the CPA (especially in China and South Korea), NAM (especially in the USA) and PAO (especially in Australia). In these regions, the economic stability and the developed energy network provide a great support in promoting solar (incl. PV/T) technologies. Therefore, clean energy supplied by solar systems on the rooftops of the abovementioned areas can be crucial in decarbonizing the building sector during the forthcoming decades. Significant increase in the potential is forecast for such developing regions as the LAC, PAS and SAS, which is in connection with the expansion of the building stock. The realization of the potential extremely depend on in what extent the new buildings will be regulated to be advanced in energy efficiency and in what extent the existing stock will be renovated and equipped with solar panels/collectors to compensate the energy demand. To reach an optimum in using solar thermal and electric energy for these purposes, both renovation and increasing energy efficiency must be aided via governmental and external subsidies. Without these incentives, there is a potential undesired outcome that the growing energy demand cannot be covered entirely by carbon-free sources. Among the regions, the AFR needs to take the longest step to be prepared for taking advantage of PV/T technology. Although most African countries show immerse solar potential being untapped, there are obvious economic and infrastructural constrains. The deployment of the estimated potential is predominantly doubtful in rural areas where the connection to the electric grid is

limited or not possible. A feasible solution for suppressing energy inequality would be the intense financial support of electricity and thermal energy technologies, but due to the high prices of such technology, their application is still a challenge in more developed regions as well.

At building level, the single and multifamily buildings were shown to have the highest rooftop PV/T potential. Their dominance is attributed to their highest share within the stock and low utilization factor. Our estimation demonstrated that the technical potential will likely to increase most dynamically for tertiary building types (especially for offices), indicating a good agreement between the regions. To maximize the future exploitation of the rooftop PV/T potential for residential buildings, the owners must be made interested in investing in green PV/T technology by overarching the initial higher costs. For tertiary buildings, the great challenge is to select the appropriate solution that fits well to the characteristics of the given building. For this reason, high-rise offices can optimize their solar energy production by installing solar systems integrated into vertical surfaces (e.g., facades) instead of limiting the utilization on rooftops. By also considering these "vertical solar energy generators", the overall building-related PV/T technical potential is even higher as compared the estimated values in our assessment.

The $E_{TH\ total\ supp}$ and $E_{EL\ total\ supp}$ is utilizable to cover partly or entirely the electric and thermal energy consumption of building occupants associated with cooling/heating, hot water production, cooking, lighting and the operation of electrical appliances. Nevertheless, the demand and supply side must be in phase to avoid the usage of additional energy sources. On a yearly scale, the energy demand of most activities, except for the cooling and heating, has minor fluctuations (Lee et al., 2014). The heating demand is mostly limited to the late autumn/early spring and winter months at middle to higher latitudes, with the exception of arid areas with high temperature range (e.g., deserts) where, however, a negligible part of the building stock is located. Fig. 8 showed that in certain regions (e.g., NAM, WEU, FSU and EEU) $E_{TH\ total\ supp}$ shows decline, falling to around its minimum during the cold period of the year. This means that there may be a significant mismatch between the production and consumption, which highlights the importance of thermal energy storage (TES) (Heier et al., 2015). Due to the penetration of phase change fluids, cool energy storage (CTES) has also been gaining interest, which can further reduce the mismatch between the supply and demand side by covering the energy consumption associated with refrigeration and air-conditioning (AC) (Sarbu and Sebarchievici, 2018). The cooling demand of buildings is mostly related to AC systems consuming electrical energy. It is an increasingly observable trend that the cooling of interiors not only the problem of regions near the Tropics, since the cooling demand and the resulting energy use have been ramping up further north due to the climate change (Spinoni et al., 2018). As it can be seen in Fig. 9a and 9b., the maximum of the $E_{EL\ total\ supp}$ is concentrated on working hours, when residential buildings have the lowest consumption during the year. However, in commercial/public buildings (e.g., offices, retails, educational buildings) the dynamics of the demand are reversed, which helps to obtain a balance between consumption and production at those building types. Furthermore, it may be beneficial in areas with higher irradiation that in the early morning and late afternoon hours, (already and still) notable production may occur, which partially coincide with consumption before and after the rush hours.

By 2022 the extrapolated rooftop PV production (assuming about one third of total production taking place on building rooftops; SolarPower Europe, 2019) will be about 0.32 PWh (IRENA, 2021). This production, therefore, is only the 1.1% of the PV/T technical potential for the $E_{EL\ total\ supp}$. Due to the historical and expected trends of the installed capacity of solar panels and collectors on residential and commercial rooftops, this ratio will likely to be closer to the actual technical potential in the following decades. In 2019, the electricity consumption by residential plus commercial and services sector was 10.9 PWh (IEA, 2021), which is 60% of the energy production can be supplied by PV/T collectors globally. In other words, approximately two thirds of the buildings should be covered by solar PV/T collectors to cover the on-site building-related electricity needs. By realizing most of the solar potential on rooftops, the competition for valuable land resources could be alleviated, while applying green energy the building-related carbon footprint could be reduced to the climate neutral level.

6. Final remarks

This study, however, fills a scientific gap and provides insightful modeling evidence on the enormous untapped technical potential of solar energy production by rooftop integrated PV/T collectors, there is a need to further promote this encouraging technology and to give widely applicable solutions for thermal and energy storage. Since the lack of incentives, limited manufacturing potential and long payback period can be considered as the most burning challenges needed to be overcome by the PV/T technology, it is also very essential to explore more of its benefits from economic and environmental point of view.

Therefore, s a further agenda, we intend to analyze the hourly outputs of solar energy supply with more focus on the financial return and CO_2 reduction potential of PV/T systems. Additionally, we plan the comparison of energy production and demand at hourly scale for each of the regions across the World to have a better perception on the net-zero and energy storage possibilities and needs of buildings. As the flexibility and the complexity of the BISE model allows and it could lead to even more robust estimations, our forthcoming studies will also prioritize simulations of solar potential undertaken at urban and neighborhood scale and supported by very high-resolution LIDAR-based rooftop information.

CRediT authorship contribution statement

Gergely Molnár: Methodology, Software, Visualization, Validation, Writing – original draft. **Diana Ürge-Vorsatz:** Conceptualization, Methodology, Writing – review & editing. **Souran Chatterjee:** Methodology, Investigation, Writing – original draft.

Declaration of competing interest

The authors declare that they have no known competing financial interests or personal relationships that could have appeared to influence the work reported in this paper.

Data availability

Data will be made available on request.

Acknowledgement

This paper is based on research conducted within the EC funded Horizon 2020 Framework Programme for Research and Innovation (EU H2020) Project titled "Sustainable Energy Transitions Laboratory" (SENTINEL)- Grant Agreement No. 837089. The authors would like to acknowledge the support from the EC. The content of the paper is the sole responsibility of its authors and does not necessarily reflect the views of the EC. We also received funding from the Energy Demand changes Induced by Technological and Social innovations (EDITS) project, which is part of the initiative coordinated by the Research Institute of Innovative Technology for the Earth (RITE) and International Institute for Applied Systems Analysis (IIASA) (and funded by Ministry of Economy, Trade, and Industry (METI), Japan). The authors would also like to express their deep gratitude to Ksenia Petrichenko for elaborating the earlier versions of the methodology and the BISE model.

Appendix A. Supplementary data

Supplementary data to this article can be found online at https://doi.org/10.1016/j.jclepro.2022.134133.

References

Babu, C., Ponnambalam, P., 2017. The role of thermoelectric generators in the hybrid PV/T systems: a review. Energy Convers. Manag. 151, 368–385. https://doi.org/10.1016/j.enconman.2017.08.060.

Bloem, J.J., Lodi, C., Cipriano, J., Chemisana, D., 2012. An outdoor test reference environment for double skin applications of building integrated PhotoVoltaic systems. Energy Build. 50, 63–73. https://doi.org/10.1016/j.enbuild.2012.03.023.

Bódis, K., Kougias, I., Jäger-Waldau, A., Taylor, N., Szabó, S., 2019. A high-resolution geospatial assessment of the rooftop solar photovoltaic potential in the European Union. Renew. Sustain. Energy Rev. 114, 109309 https://doi.org/10.1016/j.rser.2019.109309.

Brito, M.C., Gomes, N., Santos, T., Tenedório, J.A., 2012. Photovoltaic potential in a Lisbon suburb using LiDAR data. Sol. Energy 86, 283–288. https://doi.org/10.1016/j.solener.2011.09.031.

Buffat, R., Grassi, S., Raubal, M., 2018. A scalable method for estimating rooftop solar irradiation potential over large regions. Appl. Energy 216, 389–401. https://doi.org/10.1016/j.apenergy.2018.02.008.

Byrne, J., Taminiau, J., Kurdgelashvili, L., Kim, K.N., 2015. A review of the solar city concept and methods to assess rooftop solar electric potential, with an illustrative application to the city of Seoul. Renew. Sustain. Energy Rev. 41, 830–844. https://doi.org/10.1016/j.rser.2014.08.023.

Castellanos, S., Sunter, D.A., Kammen, D.M., 2017. Rooftop solar photovoltaic potential in cities: how scalable are assessment approaches? Environ. Res. Lett. 12 https://doi.org/10.1088/1748-9326/aa7857.

Chatterjee, Souran, Benedek, Kiss, Diana, Ürge-Vorsatz, Sven, Teske, 2022. Decarbonisation Pathways for Buildings. Achieving the Paris Climate Agreement Goals. Springer.

CIESIN, 2018. Gridded Population of the World (GPW), V4. National Identifier Grid. Country-Level Information and Sources Revision 11. https://sedac.ciesin.columbia.edu/binaries/web/sedac/collections/gpw-v4/gpw-v4-country-level-summary-rev11.xlsx. accessed 1.11.21.

Corbane, C., Syrris, V., Sabo, F., Politis, P., Melchiorri, M., Pesaresi, M., Soille, P., Kemper, T., 2021. Convolutional neural networks for global human settlements mapping from Sentinel-2 satellite imagery. Neural Comput. Appl. 33, 6697–6720. https://doi.org/10.1007/s00521-020-05449-7.

Deng, Y.Y., Haigh, M., Pouwels, W., Ramaekers, L., Brandsma, R., Schimschar, S., Grözinger, J., de Jager, D., 2015. Quantifying a realistic, worldwide wind and solar electricity supply. Global Environ. Change 31, 239–252. https://doi.org/10.1016/j.gloenvcha.2015.01.005.

Diwania, S., Agrawal, S., Siddiqui, A.S., Singh, S., 2020. Photovoltaic–thermal (PV/T) technology: a comprehensive review on applications and its advancement. Int. J. Energy Environ. Eng. 11, 33–54. https://doi.org/10.1007/s40095-019-00327-y.

DUALSUN, 2021. Datasheet SPRING 375 Shingle Black. https://my.dualsun.com/wp-content/uploads/sites/2/DualSun-EN-Datasheet-SPRING-375-Shingle-Black.pdf. accessed 2.13.21.

El Chaar, L., Lamont, L.A., El Zein, N., 2011. Review of photovoltaic technologies. Renew. Sustain. Energy Rev. 15, 2165–2175. https://doi.org/10.1016/j.rser.2011.01.004.

ETALAB, 2020. Building Cadastre Data of France. https://cadastre.data.gouv.fr/data/etalab-cadastre/2020-10-01/shp/departements/. accessed 12.30.20.

SolarPower Europe, 2019. Global Market Outlook for Solar Power/2019-2023. Belgium: SolarPower Europe (Schmela, M). https://www.solarpowereurope.org/global-market-outlook-2019-2023/. accessed 5.1.21.

Eyring, V., Bony, S., Meehl, G.A., Senior, C.A., Stevens, B., Stouffer, R.J., Taylor, K.E., 2016. Overview of the coupled model Intercomparison project phase 6 (CMIP6) experimental design and organization. Geosci. Model Dev. (GMD) 9, 1937–1958. https://doi.org/10.5194/gmd-9-1937-2016.

SPF FINANCES, 2020. Building Cadastre Data of Belgium. https://eservices.minfin.fgov.be/myminfin-web/pages/cadastral-plans. accessed 12.30.20.

Gelaro, R., McCarty, W., Suárez, M.J., Todling, R., Molod, A., Takacs, L., Randles, C.A., Darmenov, A., Bosilovich, M.G., Reichle, R., Wargan, K., Coy, L., Cullather, R., Draper, C., Akella, S., Buchard, V., Conaty, A., da Silva, A.M., Gu, W., Kim, G.K., Koster, R., Lucchesi, R., Merkova, D., Nielsen, J.E., Partyka, G., Pawson, S., Putman, W., Rienecker, M., Schubert, S.D., Sienkiewicz, M., Zhao, B., 2017. The modern-era retrospective analysis for research and applications, version 2 (MERRA-2). J. Clim. 30, 5419–5454. https://doi.org/10.1175/JCLI-D-16-0758.1.

Geoportal, Č.Ú.Z.K., 2020. Building Cadastre Data of Czechia. https://services.cuzk.cz/gml/inspire/cpx/epsg-4258/. accessed 12.30.20.

Grau, T., Huo, M., Neuhoff, K., 2012. Survey of photovoltaic industry and policy in Germany and China. Energy Pol. 51, 20–37. https://doi.org/10.1016/j.enpol.2012.03.082.

Gul, M., Kotak, Y., Muneer, T., 2016. Review on Recent Trend of Solar Photovoltaic Technology. Energy Exploration and Exploitation. https://doi.org/10.1177/0144598716650552.

Güneralp, B., Zhou, Y., Ürge-Vorsatz, D., Gupta, M., Yu, S., Patel, P.L., Fragkias, M., Li, X., Seto, K.C., 2017. Global scenarios of urban density and its impacts on building energy use through 2050. Proc. Natl. Acad. Sci. U.S.A. 114, 8945–8950. https://doi.org/10.1073/pnas.1606035114.

Hannah, R., Roser, M., 2020. Renewable energy. https://ourworldindata.org/renewable-energy accessed 2.14.21.

Heier, J., Bales, C., Martin, V., 2015. Combining thermal energy storage with buildings - a review. Renew. Sustain. Energy Rev. 42, 1305–1325. https://doi.org/10.1016/j.rser.2014.11.031.

Hofman, Y., de Jager, D., Molenbroek, E., Schilig, F., Voogt, M., 2002. The Potential of Solar Electricity to Reduce CO2 Emissions, vol. 106. Ecofys, Utrecht. https://ieaghg.org/docs/General_Docs/Reports/PH4-14%20Solar.pdf. accessed 4.4.2021.

Homerenergy, 2021. HOMER Grid 1.8 - User Guide. https://www.homerenergy.com/products/grid/docs/latest/index.html. accessed 1.11.21.

Hong, T., Lee, M., Koo, C., Jeong, K., Kim, J., 2017. Development of a method for estimating the rooftop solar photovoltaic (PV) potential by analyzing the available rooftop area using Hillshade analysis. Appl. Energy 194, 320–332. https://doi.org/10.1016/j.apenergy.2016.07.001.

Hoogwijk, M.M., 2004. On the Global and Regional Potential of Renewable Energy Sources. PhD Dissertation. Utrecht University, Utrecht, the Netherlands, p. 256p. https://core.ac.uk/download/pdf/39700207.pdf. accessed 4.4.21.

IDEE, 2020. Building Cadastre Data of Spain. http://www.catastro.minhap.gob.es/webinspire/index_eng.html. accessed 12.30.20.

IEA, 2020a. Tracking Buildings 2020. IEA, Paris. https://www.iea.org/reports/tracking-buildings-2020. accessed 3.11.21.

IEA, 2020b. World Energy Model. IEA, Paris. https://www.iea.org/reports/world-energy-model. accessed 3.9.21.

IEA, 2021. World Electricity Final Consumption by Sector, 1974-2019. https://www.iea.org/data-and-statistics/charts/world-electricity-final-consumption-by-sector-1974-2019. accessed 10.16.21.

INSPIRE, 2020. INSPIRE GEOPORTAL. Data Sets by Theme and Cadastral Parcels. https://inspire-geoportal.ec.europa.eu/overview.html?view=themeOverview&theme=cp. accessed 12.29.20.

IRENA, 2021. Statistics Time Series. https://www.irena.org/Statistics/View-Data-by-Topic/Capacity-and-Generation/Statistics-Time-Series. accessed 7.25.21.

Jacobson, M.Z., Jadhav, V., 2018. World estimates of PV optimal tilt angles and ratios of sunlight incident upon tilted and tracked PV panels relative to horizontal panels. Sol. Energy 169, 55–66. https://doi.org/10.1016/j.solener.2018.04.030.

Jordan, D.C., Kurtz, S.R., 2013. Photovoltaic degradation rates - an analytical review. Prog. Photovoltaics Res. Appl. 21, 12–29. https://doi.org/10.1002/pip.1182.

Joshi, S., Mittal, S., Holloway, P., Shukla, P.R., Ó Gallachóir, B., Glynn, J., 2021. High resolution global spatiotemporal assessment of rooftop solar photovoltaics potential for renewable electricity generation. Nat. Commun. 12, 1–15. https://doi.org/10.1038/s41467-021-25720-2.

JRCDC, 2020. Global Human Settlement Layers. https://data.jrc.ec.europa.eu/collection/ghsl. accessed 12.29.20.

Kambezidis, H.D., Psiloglou, B.E., 2021. Estimation of the optimum energy received by solar energy flat-plate convertors in Greece using typical meteorological years. Part I: south-oriented tilt angles. Appl. Sci. 11, 1. https://doi.org/10.3390/app11041547, 27.

Kang, J., Körner, M., Wang, Y., Taubenböck, H., Zhu, X.X., 2018. Building instance classification using street view images. ISPRS J. Photogrammetry Remote Sens. 145, 44. https://doi.org/10.1016/j.isprsjprs.2018.02.006, 59.

Kurdgelashvili, L., Li, J., Shih, C.H., Attia, B., 2016. Estimating technical potential for rooftop photovoltaics in California, Arizona and New Jersey. Renew. Energy 95, 286–302. https://doi.org/10.1016/j.renene.2016.03.105.

Lee, I.H., Ahn, Y.H., Park, J., Kim, S. Do, 2014. District energy use patterns and potential savings in the built environment: case study of two districts in Seoul, South Korea. Asian J. Atmos. Environ. 8, 48–58. https://doi.org/10.5572/ajae.2014.8.1.048.

Lopez, A., Roberts, B., Heimiller, D., Blair, N., Porro, G., 2012. U.S. Renewable energy technical potentials: a GIS-based analysis. Natl. Renew. Energy Lab. Doc. 1, 1–40.

Mainzer, K., Killinger, S., McKenna, R., Fichtner, W., 2017. Assessment of rooftop photovoltaic potentials at the urban level using publicly available geodata and image recognition techniques. Sol. Energy 155, 561–573. https://doi.org/10.1016/j.solener.2017.06.065.

Mangiante, M.J., Whung, P.Y., Zhou, L., Porter, R., Cepada, A., Campirano, E., Licon, D., Lawrence, R., Torres, M., 2020. Economic and technical assessment of rooftop solar photovoltaic potential in Brownsville, Texas, U.S.A. Comput. Environ. Urban Syst. 80, 101450 https://doi.org/10.1016/j.compenvurbsys.2019.101450.

Margolis, R., Gagnon, P., Melius, J., Phillips, C., Elmore, R., 2017. Using GIS-based methods and lidar data to estimate rooftop solar technical potential in US cities. Environ. Res. Lett. 12 https://doi.org/10.1088/1748-9326/aa7225.

McNeil, M.A., Letschert, V.E., de la Rue du Can, S., Ke, J., 2013. Bottom-Up Energy Analysis System (BUENAS)-an international appliance efficiency policy tool. Energy Effic 6, 191–217. https://doi.org/10.1007/s12053-012-9182-6.

OECD, 2021. Real GDP Lond-Term Forecast (Indicator). https://doi.org/10.1787/d927bc18-en.

Oloo, F., Olang, L., Strobl, J., 2015. Spatial modelling of solar energy potential in Kenya. Int. J. Sustain. Energy Plan. Manag. 6, 17–30. https://doi.org/10.5278/ijsepm.2015.6.3.

Oruc, M.E., Desai, A.V., Kenis, P.J.A., Nuzzo, R.G., 2016. Comprehensive energy analysis of a photovoltaic thermal water electrolyzer. Appl. Energy 164, 294–302. https://doi.org/10.1016/j.apenergy.2015.11.078.

Peng, J., Lu, L., 2013. Investigation on the development potential of rooftop PV system in Hong Kong and its environmental benefits. Renew. Sustain. Energy Rev. 27, 149–162. https://doi.org/10.1016/j.rser.2013.06.030.

Petrichenko, K., 2014. Net-Zero Energy Buildings: Global and Regional Perspectives. PhD Dissertation. Central European University, Budapest, Hungary, p. 355.

Petrichenko, K., Ürge-Vorsatz, D., Cabeza, L.F., 2019. Modeling global and regional potentials for building-integrated solar energy generation. Energy Build. 198, 329–339. https://doi.org/10.1016/j.enbuild.2019.06.024.

REN21, 2021. Renewables in Cities 2021 Global Status Report (Paris: REN21 Secretariat). https://www.ren21.net/cities-2021/. accessed 6.22.21.

Rogelj, J., Shindell, D., Jiang, K., Fifita, S., 2018. IPCC 2018, Cap2. Glob. Warm. 1.5°C. An IPCC Spec. Rep., p. 2

Romero Rodríguez, L., Duminil, E., Sánchez Ramos, J., Eicker, U., 2017. Assessment of the photovoltaic potential at urban level based on 3D city models: A case study and new methodological approach. Sol. Energy 146, 264–275. https://doi.org/10.1016/j.solener.2017.02.043.

Sampaio, P.G.V., González, M.O.A., 2017. Photovoltaic solar energy: Conceptual framework. Renew. Sustain. Energy Rev. 74, 590–601. https://doi.org/10.1016/j.rser.2017.02.081.

Sarbu, I., Sebarchievici, C., 2018. A comprehensive review of thermal energy storage. Sustain. Times 10. https://doi.org/10.3390/su10010191.

Schupfner, M., Wieners, K.-H., Wachsmann, F., Steger, C., Bittner, M., Jungclaus, J., Früh, B., Pankatz, K., Giorgetta, M., Reick, C., Legutke, S., Esch, M., Gayler, V., Haak, H., de Vrese, P., Raddatz, T., Mauritsen, T., von Storch, J.-S., Behrens, J., Brovkin, V., Claussen, M., Crueger, T., Fast, I., Fiedler, S., Hagemann, S., Hohenegger, C., Jahns, T., Kloster, S., Kinne, S., Lasslop, G., Kornblueh, L., Marotzke, J., Matei, D., Meraner, K., Mikolajewicz, U., Modali, K., Müller, W., Nabel, J., Notz, D., Peters-von Gehlen, K., Pincus, R., Pohlmann, H., Pongratz, J., Rast, S., Schmidt, H., Schnur, R., Schulzweida, U., Six, K., Stevens, B., Voigt, A., Roeckner, E., 2019. DKRZ MPI-ESM1.2-HR Model Output Prepared for CMIP6 ScenarioMIP. https://doi.org/10.22033/ESGF/CMIP6.2450.

Shin, G., Jeon, J.G., Kim, J.H., Lee, J.H., Kim, H.J., Lee, J., Kang, K.M., Kang, T.J., 2020. Thermocells for hybrid photovoltaic/thermal systems. Molecules 25. https://doi.org/10.3390/molecules25081928.

Shukla, A.K., Sudhakar, K., Baredar, P., 2017. Renewable energy resources in South Asian countries: Challenges, policy and recommendations. Resour. Technol. 3, 342–346. https://doi.org/10.1016/j.reffit.2016.12.003.

Spinoni, J., Vogt, J.V., Barbosa, P., Dosio, A., McCormick, N., Bigano, A., Füssel, H.M., 2018. Changes of heating and cooling degree-days in Europe from 1981 to 2100. Int. J. Climatol. 38, e191–e208. https://doi.org/10.1002/joc.5362.

Strzalka, A., Alam, N., Duminil, E., Coors, V., Eicker, U., 2012. Large scale integration of photovoltaics in cities. Appl. Energy 93, 413–421. https://doi.org/10.1016/j.apenergy.2011.12.033.

Svarc, J., 2021. Best Solar Inverters 2021 — Clean Energy Reviews. https://www.cleanenergyreviews.info/blog/best-grid-connect-solar-inverters-sma-fronius-solaredge-abb. accessed 5.17.21.

Trainer, T., 2017. Some problems in storing renewable energy. Energy Pol. 110, 386–393. https://doi.org/10.1016/j.enpol.2017.07.061.

TRIPLE SOLAR, 2021. Triple Solar Heat Pump Panels. https://triplesolar.eu/wp-content/uploads/2021/10/Triple-Solar-product-information-PVT-heat-pump-panels-M3-2021.pdf. accessed 2.13.21.

UN, 2018. World Urbanization Prospects 2018. Department of Economic and Social Affairs. World Population Prospects 2018. https://population.un.org/wup/Publications/Files/WUP2018-Report.pdf. accessed 1.22.21.

Urge-Vorsatz, D., Petrichenko, K., Antal, M., Staniec, M., Labelle, M., Ozden, E., Labzina, E., 2012. Best Practice Policies for Low Carbon & Energy Buildings Best Practice Policies for Low Carbon & Energy Buildings. A Scenario Analysis. Research Report Prepared by the Center for Climate Change and Sustainable Policy (3CSEP) for the Global Buildings Performance Network. https://www.gbpn.org/wp-content/uploads/2014/06/08.CEU-Technical-Report-copy_0.pdf. accessed 1.11.21.

Urge-Vorsatz, D., Khosla, R., Bernhardt, R., Chan, Y.C., Verez, D., Hu, S., Cabeza, L.F., 2020. Advances toward a net-zero global building sector. Annu. Rev. Environ. Resour. 45, 227–269. https://doi.org/10.1146/annurev-environ-012420-045843.

van de Ven, D.J., Capellan-Peréz, I., Arto, I., Cazcarro, I., de Castro, C., Patel, P., Gonzalez-Eguino, M., 2021. The potential land requirements and related land use change emissions of solar energy. Sci. Rep. 11, 1–12. https://doi.org/10.1038/s41598-021-82042-5.

Walch, A., Castello, R., Mohajeri, N., Scartezzini, J.L., 2020. Big data mining for the estimation of hourly rooftop photovoltaic potential and its uncertainty. Appl. Energy 262, 114404. https://doi.org/10.1016/j.apenergy.2019.114404.

Wiginton, L.K., Nguyen, H.T., Pearce, J.M., 2010. Quantifying rooftop solar photovoltaic potential for regional renewable energy policy. Comput. Environ. Urban Syst. 34, 345–357. https://doi.org/10.1016/j.compenvurbsys.2010.01.001.

Yang, T., Athienitis, A.K., 2016. A review of research and developments of building-integrated photovoltaic/thermal (BIPV/T) systems. Renew. Sustain. Energy Rev. 66, 886–912. https://doi.org/10.1016/j.rser.2016.07.011.

Zhang, J., Su, X., Shen, M., Dai, Z., Zhang, L., He, X., Cheng, W., Cao, M., Zou, G., 2013. Enlarging photovoltaic effect: Combination of classic photoelectric and ferroelectric photovoltaic effects. Sci. Rep. 3, 1–6. https://doi.org/10.1038/srep02109.